Nonlinear optical behavior of chloro antimony (III) hexadecafluorophthalocianinato thin films characterized by Z-scan technique

G. Mendoza-Torres[a], D. H. Cuate-Gomez[b], Y. E. Bravo-García[a], E. Reynoso-Lara[a], G. Méndez-Muñoz[c], J. L. Sosa-Sanchez[d], M. M. Mendez-Otero[c], and J. A. Dávila-Pintle[a]

[a]*Facultad de Ciencias de la Electrónica, Benemérita Universidad Autónoma de Puebla, Av. San Claudio s/n, Cd. Universitaria, Col. San Manuel, Puebla, 72570 México.*
[b]*Instituto Tecnológico Superior Progreso, ITSP, Blvd. Tecnológico de Progreso s/n, Centro, 97320 Progreso, Yucatán.*
[c]*Facultad de Ciencias Físico-Matemáticas, Benemérita Universidad Autónoma de Puebla, Av. San Claudio s/n, Cd. Universitaria, Col. San Manuel, Puebla, 72570 México.*
[d]*Centro de Investigación en Dispositivos Semiconductores, Benemérita Universidad Autónoma de Puebla, Av. San Claudio s/n, Cd. Universitaria, Col. San Manuel, Puebla, 72570 México.*

Received 23 April 2025; accepted 7 July 2025

In this work, two chloro antimony (III) hexadecafluorophthalocianinato thin films, with two different concentrations were deposited on glass substrates, Z-scan experiments at the wavelength of 633 nm (HeNe laser) and different optical powers were carried out. The results were fitted with the Photo-Induced Lens and Nonlocal theoretical models. Negative and non-local nonlinear optical response behavior is reported.

Keywords: Phthalocyanines; Z-scan; photo-induced lens; nonlocality.

DOI: https://doi.org/10.31349/RevMexFis.71.061302

1. Introduction

The metallophthalocyanines (MPcs) have garnered significant interest since their accidental discovery in the early 20th century [1]. These compounds exhibit high chemical and thermal stability, aromaticity, and synthetic flexibility [2]. Their deep, intense color has led to their use as pigments in the plastics industry and as dyes in the textile industry [3]. The structure of phthalocyanines and their strong optical absorption in the visible region, known as the Q-band, are responsible for their coloring properties [4]. The Q-band is characteristic of a macrocyclic tetrapyrrole ring with 18 delocalized electrons. The molar extinction coefficient of the Q-band of phthalocyanines varies depen-ding on the central metal and solvent [5]. For example, the molar extinction-coefficient of zinc phthalocyanine is $2.818 \times 10^5 \text{dm}^3 \cdot \text{mol}^{-1} \cdot \text{cm}^{-1}$ at 674 nm [6]. MPcs intensely absorb in the red end of the visible spectrum, and their wavelength varies depending on the central metal and substituents [7]. The presence of substituents increases solubility and reduces molecular aggregation. Recently, new antimony phthalocyanine complexes substituted with octa-phenoxy and 4-tert-butylphenoxy have been synthesized, and their photophysical and photochemical behavior has been studied [8]. These complexes exhibit unique properties, such as the formation of J-aggregates and the oxidation of antimony under visible irradiation. However, their behavior in the triplet state has not been explored yet [9].

Conjugated organic molecules, such as phthalocyanines, possess third-order nonlinear optical properties [10], making them suitable for applications such as optical processing [11] and optical limiting [12]. However, their insolubility in common solvents is a major obstacle. The incorporation of peripheral and non-peripheral substituents can improve solubility [13].

Phthalocyanines have a high structural flexibility and can accommodate approximately 70 different elements in their central cavity. Their high nonlinearity is due to the delocalized π-electrons. These properties make them suitable for applications in photonics and biomedicine [14]. The chloro antimony (III) hexadecafluorophthalocianinato compound (F_{16}SbPcCl) consists of a perfluorinated phthalocyanine ring coordinated to an antimony (III) ion and a chlorine ligand. The perfluorination of the phthalocyanine ring confers unique properties, such as enhanced thermal and an increased solubility [9,15].

The Z-scan technique, developed by Sheik-Bahae and collaborators in 1989 [16], is a fundamental tool for characterizing the nonlinear optical properties of various materials. This technique stands out for its ability to measure both nonlinear absorption and refraction coefficients using a single laser beam with high sensitivity and precision. The simplicity and effectiveness of the Z-scan technique have allowed it to be adopted in a wide range of studies, including the characterization of antimony phthalocyanines. The objective of this work is to study the nonlinear optical behavior of antimony phthalocyanines deposited on glass using the Z-scan technique. Specifically, we aim to characterize and compare the nonlinear properties of the F0-F_{16}SbPcCl and F1-F_{16}SbPcCl samples, analyzing differences in their optical responses under varying laser powers. With the help of two theoretical

models, that reproduce the Z-scan curves, this study seeks to provide some of the nonlinear optical properties most important of these samples to their possible applications in optoelectronics and photodynamic therapy.

2. Experimental section

2.1. Synthesis of chloro antimony (III) hexadecafluorophthalocianinato (F_{16}SbPcCl)

Under a nitrogen atmosphere and with magnetic stirring, a reaction was carried out between 100 mg (0.5 mmol) of tetrafluorophthalonitrile (TFPN) and 22.8 mg (0.1 mmol) of antimony trichloride that had been freshly dried at 140°C for 90 minutes. The reaction was carried out at 200°C for 20 minutes with gentle stirring. Upon cooling, a solid was obtained and it was whashed with ethanol to dissolve traces of metal salt, and subsequently it was filtered. The resulting product, F_{16}SbPcCl, is a deep blue-black powder, soluble in chlorinated solvents, acetone, and ethyl acetate.

2.2. Dilution of F_{16}SbPcCl with methanol (MeOH)

To dilute F_{16}SbPcCl, a base solution (BS - F_{16}SbPcCl) was prepared using 10 mg of F_{16}SbPcCl and 100 ml of methanol (MeOH). The reagents were mixed in an Erlenmeyer flask and then subjected to an ultrasonic bath for 10 minutes. The base solution was labeled F0-F_{16}SbPcCl and it was diluted with methanol adding a 10% of the total volume of the base solution; that is, the second sample only has 9 ml of the base solution and 1 ml of MeOH and was labeled as F1-F_{16}SbPcCl (See Table I).

The glass substrates were prepared by cleaning them sequentially with xylene, acetone and methanol, followed by ultrasonication for 10 minutes in each solvent. The deposition of the samples onto the glass substrates using the drop-casting technique was carried out with an adjustable volume micropipette (ranging from 100 to 1000 μl). A volume of 150 μl of F0-F_{16}SbPcCl and F1-F_{16}SbPcCl solutions was used to obtain samples onto corning glass. A hot plate set at 45°C was employed to ensure the evaporation of the solvents, leaving behind only the thin films of F_{16}SbPcCl.

2.3. Experimental setup

Experiments using the Z-scan technique were performed on F0-F_{16}SbPcCl and F1-F_{16}SbPcCl samples to determine their nonlinear optical behavior. The experimental setup includes a HeNe laser operating at 633 nm, and a positive lens with a focal length of 5 cm, which produced a beam waist of $w_0 = 26$ μm and a depth of focus of $2z_0 = 6.7$ mm. The transmittance of the sample was measured on-axis as it was scanned through the region of highest irradiance. The photodetector was placed 80 cm from the lens, ensuring the far field condition ($z \gg z_0$).

TABLE I. Samples labels the F_{16}SbPcCl solutions.

Samples labels	Dilutions
F0-F_{16}SbPcCl	10 ml BS-F_{16}SbPcCl + 0 ml MeOH
F1-F_{16}SbPcCl	9 ml BS-F_{16}SbPcCl + 1 ml MeOH

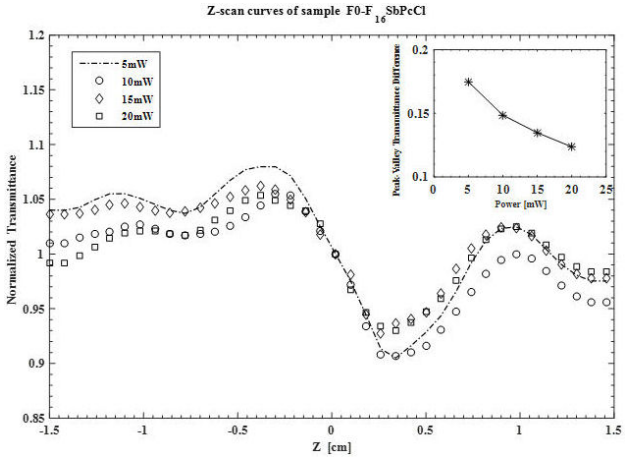

FIGURE 1. Z-scan curves for the F0-F_{16}SbPcCl sample at powers of 5, 10, 15 and 20 mW. The inset in the upper-right corner shows the evolution of ΔT_{pv} as a function of power.

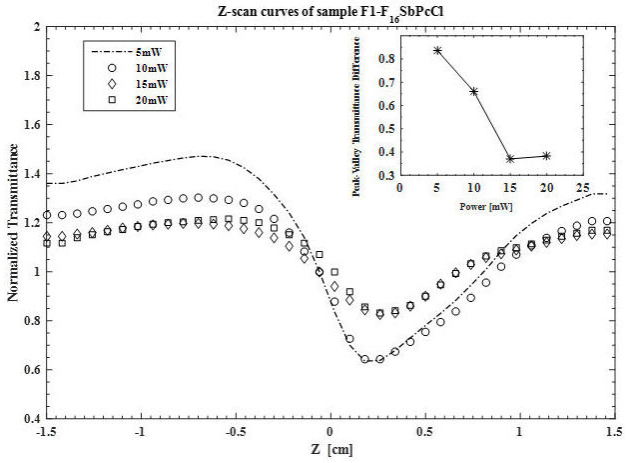

FIGURE 2. Z-scan curves for the F1-F_{16}SbPcCl sample at powers of 5, 10, 15 and 20 mW. The inset in the upper-right corner shows the evolution of ΔT_{pv} as a function of power.

Five measurements were taken for each sample varying the laser power at 1, 5, 10, 15 and 20 mW. Notably, at 1 mW, the samples did not exhibit nonlinear optical behavior. Figures 1 and 2 show the sets of Z-scan curves for the F0-F_{16}SbPcCl and F1-F_{16}SbPcCl samples, respectively. These curves are presented in normalized form, with the normalization criterion being the transmittance value at the focus. In each figure, the insets in the upper-right corner shows the evolution of the peak-to-valley amplitudes (ΔT_{pv}) of the experimental curves.

3. Results and discusions

From Figs. 1 and 2, it can be observed that both samples exhibit negative nonlinear optical behavior at this wavelength. The curve with the highest amplitude appeared at a power of 5 mW for both samples. The shape of the Z-scan curves for the F0-F_{16}SbPcCl sample differs from that of the F1-F_{16}SbPcCl sample. Specifically, the first group of curves shows a double prefocal peak that diminishes as the incident power increases. Furthermore, after reaching a minimum transmittance postfocal, the curves recover to a second maximum transmittance value, which does not get the initial maximum and then gradually declines. In contrast, curves of the sample F1-F_{16}SbPcCl are smoother, exhibiting a single prefocal peak (maximum transmittance) followed by a minimum transmittance that recovers to the transmittance value prior to the depth of focus, without reaching a second maximum, as observed in the first group of curves of sample F0-F_{16}SbPcCl. The transmittance difference between the peak and valley ($\Delta T_{pv} = |T_{\max} - T_{\min}|$) is an important parameter in analyzing Z-scan curves. It reflects the amplitude change of the curve as a function of power. The insets in Figs. 1 and 2 reveal that as the beam power increases, ΔT_{pv} decreases. For the F0-F_{16}SbPcCl sample, the decrease in ΔT_{pv} is slow and nearly linear. However, for the F1-F_{16}SbPcCl sample, the decrease is faster, and the last two ΔT_{pv} values at powers of 15 and 20 mW are almost equal, possibly due to absorption saturation in the sample. Another critical parameter is the difference in the positions of the peak and valley ($\Delta Z_{pv} = |Z_{\max} - Z_{\min}|$). Figures 1 and 2 show that the ΔZ_{pv}values are smaller for the F0-F_{16}SbPcCl sample compared to the F1-F_{16}SbPcCl sample. The average ΔZ_{pv} values were calculated as 6.8 mm for F0-F_{16}SbPcCl and 8.8 mm for F1-F_{16}SbPcCl.

3.1. Theoretical models for fitting experimental curves

Each of the experimental Z-scan curves was fitted with two theoretical models, which generated the transmittance equation of the sample in the far field. The first is the Photo-Induced Lens (PIL) model. This model considers that a lens is photo-induced in the sample when scanned in the high-intensity region of the highly focused laser beam in the Z-scan experiment. With this model, the nature of the phenomenological process that generates this photo-induced lens can be obtained. The second model considers the dimension of the material response, especially the nonlinear radial phase shift, due to the irradiance distribution of the beam on the sample; with this model, the locality of the nonlinear response can be obtained. Next a brief description of these two models is given.

3.2. Photo-Induced lens model

As mentioned above, this model considers that a lens is photo-induced in the sample due to the Gaussian nature of the irradiance of the incident beam [17]. The on-axis transmittance of the sample measured in the far field ($z \gg z_0$) depends on the focal length (F) of the photo-induced lens, as well as the Rayleigh range z_0, Eq. (1),

$$T = \frac{F^2}{z_0^2 + (F - z)^2}. \tag{1}$$

This focal length is a function of the beam radius raised to an integer power m, Eq. (2),

$$F = a_m w^m(z), \tag{2}$$

where a_m is a constant that includes the physical parameters of the sample. The units of a_m are appropriate for F to have units of length and $w(z)$ is the beam radius, Eq. (3),

$$w(z) = w_0 \left(1 + \left[\frac{z}{z_0}\right]^2\right)^{\frac{1}{2}}. \tag{3}$$

By substituting Eq. (2) and (3) into equation 1, what is called the complete transmittance formula for the photo-induced lens model is obtained, Eq. (4),

$$T = \frac{1}{1 - \frac{4x}{(1+x^2)^2}(\Delta\Phi_{0m}) + \frac{4}{(1+x^2)^3}(\Delta\Phi_{0m})^2}, \tag{4}$$

where $x = z/z_0$, $\Delta\Phi_{0m} = (z_0/2F_{0m})$ is the on axis nonlinear phase shift, and $F_{0m} = a_m w_0^m$ is the shortest photo-induced focal length. To generate theoretical transmittance curve that fits an experimental curve, the values of the parameters *m* and $\Delta\Phi_{0m}$ in equation 4 must be changed.

3.3. Non-locality model of the nonlinear response

This model considers the magnitude of the nonlinear response in the sample. This response is observed in the nonlinear phase shift on the beam, due to the change in the refractive index of the material, which is a function of the beam intensity [18]. If this nonlinear phase shift is equal to the irradiance distribution of the beam, the response is considered local; however, if the phase shift is greater or less than the beam irradiance, the nonlinear response is considered nonlocal. The most important parameters to vary in this model, to reproduce the experimental transmittance curves in the Z-scan technique, are in the phase that the beam undergoes at the exit of the sample and the parameter s; Eq. (5),

$$\Delta\Phi = \Delta\phi_0^{NL} exp\left(\frac{-sr^2}{w^2}\right) \tag{5}$$

where $\Delta\phi_0^{NL}$ is the on-axis maximum nonlinear phase shift at $z = 0$. The parameter *s* in Eq. (5) provides the value of the spatial effect in the sample, being a local value for $s = 2$ and with $s \neq 2$ it is a non-local effect. Note in Eq. (5) that the phase shift has a Gaussian distribution in which the parameter *s* modifies its width. The parameters to vary in this model are $\Delta\phi_0^{NL}$ and *s*. Figures 3 and 4 show the fit of the experimental curves for the samples F0-F_{16}SbPcCl and F1-F_{16}SbPcCl, respectively, with the two models PIL and NL.

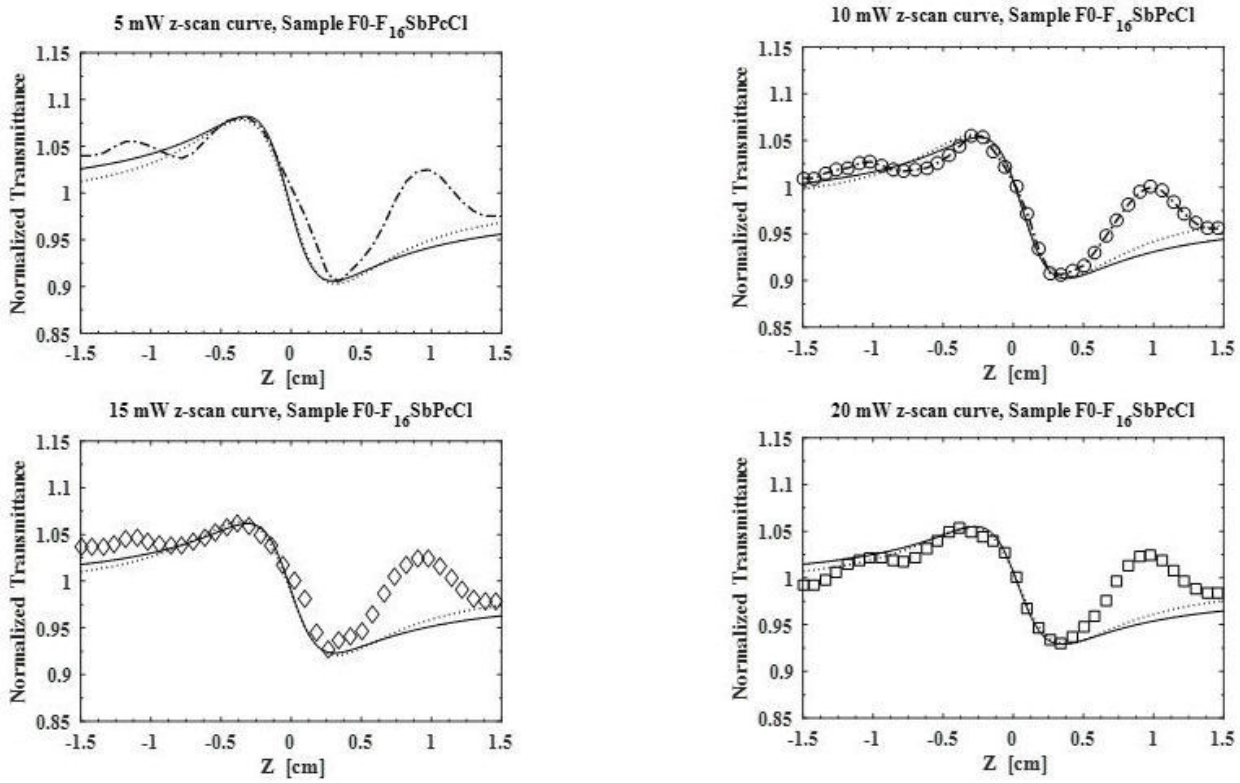

FIGURE 3. Z-scan experimental curves for F0-F_{16}SbPcCl at powers of 5, 10, 15 and 20 mW fitted with PIL (solid line) and NL (dotted line) models.

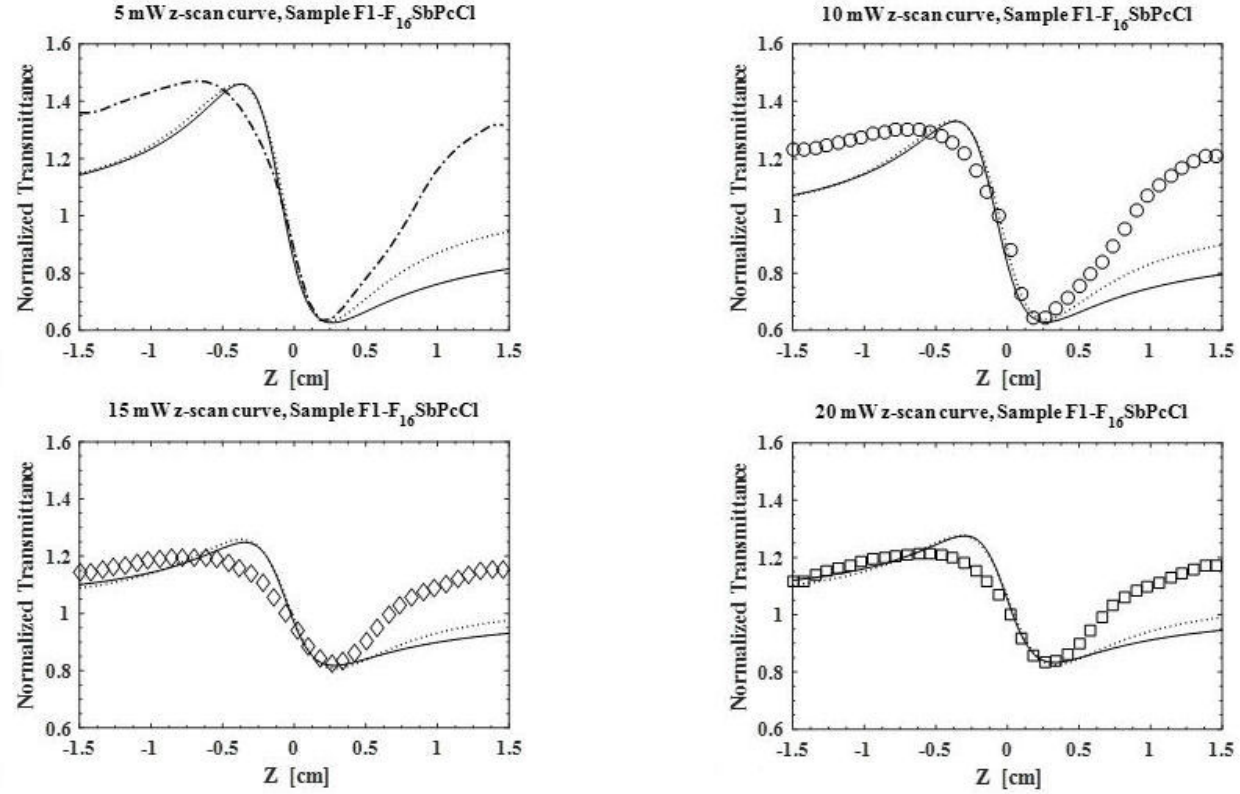

FIGURE 4. Z-scan experimental curves for F1-F_{16}SbPcCl at powers of 5, 10, 15 and 20 mW fitted with PIL (solid line) and NL (dotted line) models.

3.4. Numerical results

In Fig. 3, all curves are presented on the same scale, which is that of the experimental curve with the maximum peak-valley excursion; the same applies to Fig. 4. It is important to mention that with the two models, PIL and NL, to fit the experimental curves, better reproductions can be obtained, but only for a part of the experimental curve; that is, either the peak or the valley can be reproduced, but not both simultaneously. Therefore, the criterion chosen for fitting the curves in Figs. 3 and 4 was to match the maximum amplitudes of the numerical transmittances (peak-valley) with those of the experimental peak-valley transmittances. In the PIL model, once the best values of the parameters m and $\Delta\Phi_{0m}$ that fit the experimental curves were found, the values of the parameters a_m and F_{0m} were calculated. The values of these parameters, along with the values s and $\Delta\Phi_0^{NL}$ of the NL model that best fit the experimental curves of the samples F0-F_{16}SbPcCl and F1-F_{16}SbPcCl are shown in Tables II and III, respectively.

Tables II and III show the values of the parameters obtained with the PIL and NL models. These values are accompanied by their respective units. The constant a_m, it is function of the parameter m. In this case, since the best fit value was $m = 2$, then $a_m = a_2$, which will have units of $[m^{-1}]$.

TABLE II. Parameters values obtained with PIL and NL Models for sample F0-F_{16}SbPcCl.

		Photo-Induced Lens Model			No Local Model	
Power [mW]	m	$\Delta\Phi_0^{PIL}$ [mrad]	a_m	F_0 [mm]	$\Delta\phi_0^{NL}$ [mrad]	s
5	2	-14π	-5.65×10^5	-35.3	-98π	1
10	2	-12π	-6.59×10^5	-41.2	-85π	1
15	2	-11π	-7.19×10^5	-44.9	-80π	1
20	2	-10π	-7.91×10^5	-49.4	-70π	1

TABLE III. Parameters values obtained with PIL and NL Models for sample F1-F_{16}SbPcCl.

		Photo-Induced Lens Model			No Local Model	
Power [mW]	m	$\Delta\Phi_0^{PIL}$ [mrad]	a_m	F_0 [mm]	$\Delta\phi_0^{NL}$ [rad]	s
5	2	-65π	-1.21×10^5	-7.6	-0.45π	1
10	2	-55π	-1.43×10^5	-8.9	-0.38π	1
15	2	-34π	-2.32×10^5	-14.5	-0.25π	1
20	2	-35π	-2.26×10^5	-14.1	-0.25π	1

4. Conclusions

From the graphs in Figs. 3 and 4, it can be observed that all curves exhibit a negative nonlinear optical behavior, which implies that the photo-induced lens was divergent and consequently the shortest photo-induced focal length F_{0m} is negative, as seen in Tables II and III. According to the approximation $F \geq z_0$ written in [17], it can be said that the photo-induced lenses in the samples are weak lenses. Additionally, all curves were fitted with the same value of $m = 2$, this implies that the physical mechanism that generates the nonlinearity is thermal as indicated in [17].

The on-axis nonlinear phase shift $\Delta\Phi_{0m}$ was much less than π in all cases $\Delta\Phi_{0m} \ll \pi$ for both models. The values reported in these tables for the parameter s imply that both samples exhibit non-local nonlinearity; that is, they have a spatial affectation on the refractive index greater than the spatial distribution of the incident beam $s < 2$. Considering that in the PIL model, the difference in the positions of the peak and the valley Δz_{pv} varies as a function of the parameter m, as $\Delta z_{pv} = (2/\sqrt{m-1})z_0$; and since all curves were fitted with the value $m = 2$; therefore, the theoretical difference in the positions of the peak and the valley is $\Delta z_{pv} = 2z_0 = 6.7$ mm. From Figs. 1 and 2, the difference in the positions of the peak-valley is: 6.8 mm and 8.8 mm, respectively. It can be concluded that there is an excellent agreement between theoretical and experimental values. As reported in Ref. [19], the PIL and NL models are equivalent, which can be observed in the fits in Figs. 3 and 4. The idea of using these two models to fit the experimental curves is because they complement each other by allowing us to obtain different parameter values.

1. A. Braun and J. Tcherniac, Über die Produkte der Einwirkung von Acetanhydrid auf Phthalamid, Berichte der deutschen chemischen *Gesellschaft* **40** (1907) 2709, https://doi.org/10.1002/cber.190704002202.
2. H. Bushnaq *et al*., Phthalocyanine-enabled technologies for water treatment and disinfection strategies, *Journal of Water Process Engineering* **65** (2024) 105861, https://doi.org/10.1016/j.jwpe.2024.105861.
3. C. Verma *et al*., Phthalocyanine, naphthalocyanine and their derivatives as corrosion inhibitors: *A review, J. Mol. Liq.* **334** (2021) 116441, https://doi.org/10.1016/j.molliq.2021.116441.
4. M.Wang and K. Ishii, Photochemical properties of phthalocyanines with transition metal ions, *Coord Chem Rev* **468** (2022) 214626, https://doi.org/10.1016/j.ccr.2022.214626.
5. A. Günsel *et al*., Synthesis of non-peripherally tetrasubstituted copper (II) phthalocyanines: characterization, optical and surface properties, fabrication and photo-electrical properties of a

photosensitive diode, *Dalton Trans.* **48** (2019) 14839, https://doi.org/10.1039/C9DT02868D.

6. A. Ogunsipe, D. Maree, and T. Nyokong, Solvent effects on the photochemical and fluorescence properties of zinc phthalocyanine derivatives, J Mol Struct **650** (2003) 131, https://doi.org/10.1016/S0022-2860(03)00155-8.
7. M. Pişkin, O. F. Ozturk, and Z. Odabaş, Determination of photophysical, photochemical and spectroscopic properties of novel lead (II) phthalocyanines, *Polyhedron* **182** (2020) 114480, https://doi.org/10.1016/j.poly.2020.114480.
8. R. Kubiak and J. Janczak, Synthesis, Structure, and UV-Vis Characterization of Antimony (III) Phthalocyanine: [(SbPc)$_2$(Sb_2I_8)($SbBr_3$)]$_2$, *Molecules* **27** (2022) 1839, https://doi.org/10.3390/molecules27061839.
9. D. K. Modibane and T. Nyokong, Synthesis, photophysical and photochemical properties of octa-substituted antimony phthalocyanines, *Polyhedron* **28** (2009) 479, https://doi.org/10.1016/j.poly.2008.11.052.
10. S. V. Rao *et al*., Ultrafast nonlinear optical properties of alkylphthalocyanine nanoparticles investigated using Z-scan technique, *J Appl Phys* **105** (2009) 3079801 https://doi.org/10.1063/1.3079801.
11. H. Zhang *et al*., Phthalocyanine covalent frameworks doped in PMMA matrix as high performance nonlinear optical limiter, *Dyes and Pigments* **219** (2023) 111553, https://doi.org/10.1016/j.dyepig.2023.111553.
12. H. Lu and N. Kobayashi, Optically Active Porphyrin and Phthalocyanine Systems, *Chem. Rev.* **116** (2016) 6184, https://doi.org/10.1021/acs.chemrev.5b00588.
13. M. Kocak et al., Synthesis and comparison of the performance of two different water-soluble phthalocyanine based electrochemical biosensor, *Bioelectrochemistry* **160** (2024) 108788, https://doi.org/10.1016/j.bioelechem.2024.108788.
14. O. A. Hamad, R. O. Kareem, and P. K. Omer, Recent Developments in Synthesize, Properties, Characterization, and Application of Phthalocyanine and Metal Phthalocyanine, *J. Chem. Rev.* **6** (2024) 39, https://doi.org/10.48309/jcr.2024.412899.1250.
15. H. Isago and Y. Kagaya, Facile Antimony(V/III) Interconversion in Phthalocyanine Complexes, *Chem. Lett.* **35** (2006) 8, https://doi.org/10.1246/cl.2006.8.
16. M. Sheik-Bahae *et al*., Sensitive measurement of optical nonlinearities using a single beam, *IEEE J Quantum Electron* **26** (1990) 760, https://doi.org/10.1109/3.53394
17. E. Reynoso-Lara *et al*., Influence of the photoinduced focal length of a thin nonlinear material in the Z-scan technique, *Opt. Express* **15** (2007) 2517, https://doi.org/10.1364/OE.15.002517.
18. E. V. Garcia-Ramirez *et al*., Z-scan and spatial self-phase modulation of a Gaussian beam in a thin nonlocal and nonlinear media, *J. Opt.* **13** (2011) 085203, https://doi.org/10.1088/2040-8978/13/8/085203.
19. I. Severiano-Carrillo *et al*., Comparison of different models employed to describe the z-scan curves for thick nonlinear optical media, *J. Mod. Opt.* **60** (2013) 248, https://doi.org/10.1080/09500340.2013.769639.